2015 IEEE/RSJ International Conference on Intelligent Robots and Systems (IROS)
Congress Center Hamburg
Sept 28 - Oct 2, 2015. Hamburg, Germany

HippoCampus: A Micro Underwater Vehicle for Swarm Applications

Axel Hackbarth, Edwin Kreuzer and Eugen Solowjow

***Abstract*— The HippoCampus platform is a low-cost micro autonomous underwater vehicle for swarm robotics research. This paper presents the hardware and software design, the communication link, instrumentation, and control system. The quadrotor design enables the vehicle to perform agile maneuvers in a very confined test tank. Vehicle navigation is based on the on-board sensor suite. Autonomous path following is presented and experimental results are evaluated.**

I. INTRODUCTION

We present a novel autonomous underwater vehicle (AUV) design, which is highly maneuverable and is capable of autonomous operations using on-board processing. Our key contribution is a compact, low cost (current cost of material is approx. 600 USD) design pattern which is optimized for scaling to swarm applications, see Figures 1 and 2. Since the presented platform is significantly smaller than current underwater vehicles with this degree of autonomy, multi-vehicle operations are possible in experimental test tanks, which is an important feature for initial testing and development in the area of underwater swarm robotics research.

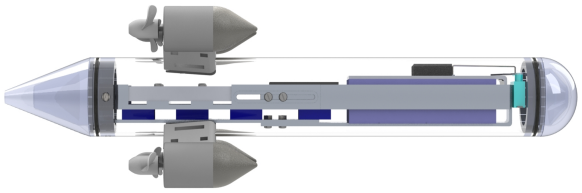

Fig. 1. Concept drawing of HippoCampus.

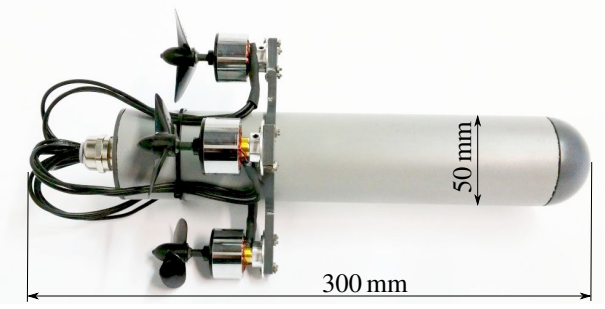

Fig. 2. Photo of functional prototype of HippoCampus.

*Research supported by the German Research Foundation (DFG) under the grant 250508151 titled “Fluid field estimation and source localization by dynamic positioning of autonomous underwater sensor nodes”.

All authors are with the Institute of Mechanics and Ocean Engineering, Hamburg University of Technology, Germany. {axel.hackbarth, kreuzer, eugen.solowjow}@tuhh.de

A. Collaborative Flow Analysis

The development of the vehicle design is driven by the goal to use multi-AUV swarm systems to analyze flow fields. In order to address the need for a controlled research environment, the presented AUV has been developed. The vehicles will measure scalar as well as vector fields and communicate sensor values to a centralized data assimilation unit which uses a computational fluid dynamics (CFD) model to replicate the marine environment. This allows the modeling of realistic environmental dynamics by the simulation of the flow field and an estimation of sinks, sources (of heat, pollution, etc.) and boundary conditions. Also, the results from the fluid dynamics simulation are fed back into the path planner for the AUVs. Depending on the mission objectives, regions with a high likelihood for sources can be of higher or lower interest as regions with a high uncertainty. While the presented vehicle design already possesses all sensors and hardware components required for inertial navigation and communication, updates of the absolute position are not available to the vehicle yet. A localization system is in development, where submerged sound sources emit acoustic signals into the water environment and each vehicle is able to perform on-board localization based on an algorithm exploiting time delay estimation via cross correlation. Since all processing is on-board, the number of vehicles is not limited by communication bandwidth as would be the case with an external camera system.

B. Related Work

Current AUVs used for research on multi-vehicle coordination are larger and more expensive than the one presented in this work. They often follow a ”classical” design approach with one propeller for propulsion and rudders, which is more streamlined and efficient, but less maneuverable in confined spaces. In general, experimental test beds for underwater swarm robotics research have been very limited so far. A test bed for multi-vehicle control research was established by the Laboratrio de Sistemas e Tecnologias Subaquticas (LSTS) at University of Porto [1]. However, the current Light Autonomous Underwater Vehicle (LAUV) designed by LSTS, with a length of 110 cm and a weight of 18 kg, is still too big to be used in experimental test tanks and too costly to be scaled to large swarms. One of the first experimental testing beds for cooperative control of underwater vehicles was developed and implemented at the University of Washington. Autonomous fin-actuated vehicles with wireless underwater communication were designed and are presented in [2]. Further AUV designs for test tank experiments in the area of collective motion are reported in [3]–[5]. Open

water applications of underwater multi-vehicle control are presented in [6], where gliders are deployed as vehicles.

The authors are convinced that recent advances in the area of micro air vehicles (MAVs) can be beneficial for the design of micro autonomous underwater vehicles. Therefore, the presented work is influenced by the rapid development, miniaturization, and high agility of MAVs and the design patterns applied in that area [7]–[10].

II. VEHICLE DESIGN

The HippoCampus design was developed from scratch with underwater swarm applications in mind. The system follows the requirements of being low cost, open source and having widely available components. A high maneuverability was emphasized during the design phase. The initial application environments are laboratory freshwater tanks with water depths of up to 10 m. However, operations in saline water are intended as well. In order to achieve a wide propagation of our system within the community and a rapid development pace, we use the PX4 framework, an open-source, open-hardware platform for mobile autonomous systems [10].

A. Mechanical Structure and Components

The HippoCampus vehicle consists of a central, cylindrical tube. This base unit hosts the electronics, battery and the microcontroller board. The cylindrical tube is designed to withstand a relative pressure of 1 bar and to provide rigidity to the vehicle. It is enclosed by two covers which provide the sealing of the base unit. The back unit passes the power cables for the four brushless DC motors and also hosts a pressure sensor. The front cover can be equipped with additional sensors. The four brushless DC motors are connected to an annulus frame which is mounted on the central tube. The four-propeller design is inspired by recent advances in the field of multi-rotor MAVs, allowing great maneuverability. Furthermore, turning rates are independent of forward motion, which is an advancement to "classic" designs with one propeller and rudders. HippoCampus does not have a dive tank. The vehicle design has neutral net buoyancy, whereby the center of volume coincides with the center of mass. The total weight of the vehicle is 700 g and it has a length of 300 mm.

B. Pixhawk Controller Board

The on-board controller board offers the functionality which is required for autonomous operations. The Pixhawk controller board was chosen as the main processing unit, mainly because it is open source, compact and provides enough computing power. It is primarily developed for micro air vehicle (MAV) systems by the PX4 project, coordinated by ETH Zurich [10]. We extend the functionality to underwater vehicles. The Pixhawk unit coordinates communication, sensing, estimation and control on-board of HippoCampus. It consists of a 168 MHz Cortex M4F CPU with 256 KB RAM and 2 MB flash memory. Data can be logged on a microSD-card.

C. Sensors and Electronics

The current sensor suite consists of the on-board Pixhawk sensors, and includes a 16 bit three-axis gyroscope and a combined a 14 bit three-axis accelerometer and magnetometer. An additional pressure sensor for depth control is installed. Other sensors, such as a temperature sensors, can be easily added. We use off the shelf electronic speed controllers (ESCs) rated at 10 Amps. The brushless DC motors are equipped with counter-rotating propellers. The vehicle is powered by a lithium iron phospate ($LiFePO_4$) battery, which has a capacity of 1800 mAh. This allows for an operational time of approximately 60 minutes. The communication link to the ground station and to other vehicles is established through radio modules from 3D Robotics. We use a carrier frequency of 433 MHz with an adjustable output power of up to 100 mW and frequency shift keying (FSK) modulation. The advantage of FSK modulation over on-off keying (OOK) for underwater communication was one of the findings in [11]. Due to attenuation of electromagnetic waves in water only short range communication can be achieved with RF. We can maintain a reliable communication link to the vehicle while it is at any point of our testing tank ($4\,\text{m} \times 3\,\text{m} \times 1.5\,\text{m}$) with an output power of 10 mW and a baud-rate of 56 700 Bd. Reducing the baud-rate and increasing the output power will increase the communication range for operations in larger testing tanks. Figure 3 provides an overview of the sensors and electronic components of the vehicle. Note, in the current development state of the vehicle the microphone for global position update is not implemented yet.

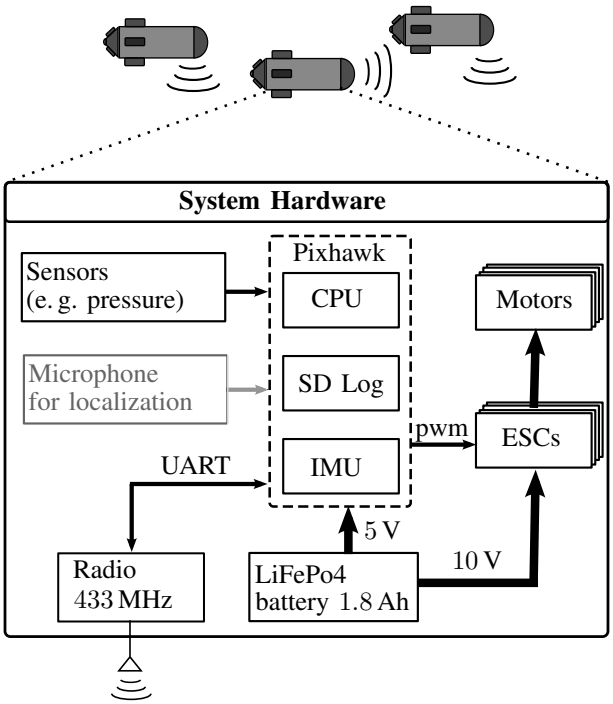

Fig. 3. Electronic components of HippoCampus. The microphone for absolute localization is not implemented yet.

D. Software Architecture

The software architecture of HippoCampus consists of three layers, see Figure 4. The Pixhawk controller board runs NuttX, a real-time operating system with a small footprint providing a POSIX-style environment. The low level drivers are implemented in NuttX. On top of NuttX the PX4 middleware provides device drivers and an object request broker (uORB) for asynchronous communication between the individual tasks. It is a node-based multi-threaded open source framework developed along the Pixhawk controller board for deeply embedded mobile robotics applications [10]. The control stack developed for HippoCampus is a customized application which runs the controller and estimator and coordinates other processes such as the user-vehicle interaction.

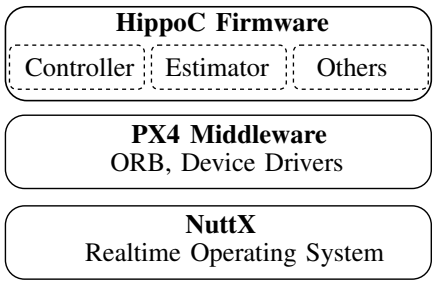

Fig. 4. Software architecture layers of HippoCampus.

III. DYNAMICS

The nonlinear dynamics are derived in North-East-Down (NED) inertial coordinates and in body fixed coordinates. The nomenclature is based on [12]. The unit vectors $\{\boldsymbol{e}_\mathrm{N}, \boldsymbol{e}_\mathrm{E}, \boldsymbol{e}_\mathrm{D}\}$ describe the inertial frame $\{\mathcal{I}\}$ and $\{\boldsymbol{x}_\mathrm{B}, \boldsymbol{y}_\mathrm{B}, \boldsymbol{z}_\mathrm{B}\}$ the body fixed frame $\{\mathcal{B}\}$ with the origin in the center of buoyancy of the vehicle, as defined in Figure 5. Let $\boldsymbol{v} = [u\ v\ w]^\intercal$ be the linear velocity and $\boldsymbol{\omega} = [p\ q\ r]^\intercal$ the

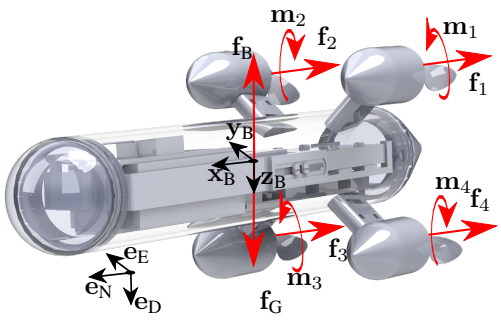

Fig. 5. Free body diagram of HippoCampus without hydrodynamic forces and moments.

angular velocity of the vehicle in the body fixed frame, which are combined to $\boldsymbol{\nu} = [\boldsymbol{v}\ \ \boldsymbol{\omega}]^\intercal$. The vector $\boldsymbol{p} = [N\ E\ D]^\intercal$ defines the position vector from the origin of $\{\mathcal{I}\}$ to the origin of $\{\mathcal{B}\}$ and the orientation vector $\boldsymbol{\Theta} = [\phi\ \theta\ \psi]^\intercal$ describes the vehicle orientation with Euler angles.

If the position and orientation of the vehicle are combined in the vector $\boldsymbol{\eta} = [\boldsymbol{p}\ \ \boldsymbol{\Theta}]^\intercal$, the kinematics for the vehicle read

$$\begin{bmatrix} \dot{\boldsymbol{p}} \\ \dot{\boldsymbol{\Theta}} \end{bmatrix} = \begin{bmatrix} \boldsymbol{R}(\boldsymbol{\Theta}) & \boldsymbol{0} \\ \boldsymbol{0} & \boldsymbol{T}(\boldsymbol{\Theta}) \end{bmatrix} \begin{bmatrix} \boldsymbol{v} \\ \boldsymbol{\omega} \end{bmatrix} \tag{1}$$

$$\Leftrightarrow \dot{\boldsymbol{\eta}} = \boldsymbol{J}(\boldsymbol{\eta})\boldsymbol{\nu}. \tag{2}$$

where $\boldsymbol{R}(\boldsymbol{\Theta})$ is the rotation tensor and $\boldsymbol{T}(\boldsymbol{\Theta})$ the angular velocity transformation tensor.

The body fixed velocities evolve according to the equation of motion

$$\boldsymbol{M}\dot{\boldsymbol{\nu}} + \boldsymbol{C}(\boldsymbol{\nu})\boldsymbol{\nu} + \underbrace{\boldsymbol{M}_A\dot{\boldsymbol{\nu}} + \boldsymbol{C}_A(\boldsymbol{\nu})\boldsymbol{\nu} + \boldsymbol{D}_A(\boldsymbol{\nu})\boldsymbol{\nu}}_{\text{hydrodynamic loads}} + \underbrace{\boldsymbol{g}(\boldsymbol{\eta})}_{\text{hydrostatic load}} = \boldsymbol{\tau}. \tag{3}$$

The matrices $\boldsymbol{M}$ and $\boldsymbol{C}$ consider the inertia and Coriolis rigid body effects respectively. The hydrodynamic loads consist of the added mass matrix $\boldsymbol{M}_\mathrm{A}$, the added Coriolis matrix $\boldsymbol{C}_\mathrm{A}$ and the added damping matrix $\boldsymbol{D}_\mathrm{A}$. The former two are due to the motions of the fluid and the latter describes the hydrodynamic damping. The hydrodynamic values are usually determined experimentally. The hydrostatic term $\boldsymbol{g}(\boldsymbol{\eta})$ considers the forces due to gravity $\boldsymbol{f}_\mathrm{G}$ and buoyancy $\boldsymbol{f}_\mathrm{B}$. Both act in $\boldsymbol{e}_\mathrm{D}$-direction. The dynamics of the vehicle can be controlled by the four propellers. The thrust forces and moments of the individual motors are denoted with $\boldsymbol{f}_i$ and $\boldsymbol{m}_i$. The control input can be written as

$$\boldsymbol{\tau} = \sum_{i=1}^{4} \begin{bmatrix} \boldsymbol{f}_i \\ \boldsymbol{m}_i + \boldsymbol{r}_i \times \boldsymbol{f}_i \end{bmatrix}, \tag{4}$$

where $\boldsymbol{r}_i$ is the position vector from the center of mass to the i-th motor.

IV. CONTROLS

For basic flight maneuvers, the dynamics of an aerial quadrotor vehicle can be easily decoupled to control the height by vertical thrust and planar motion by differential thrust of opposite rotor pairs [7]. So, within the limits of the actuators, any path in a Cartesian space can be directly followed by such a vehicle.

In contrast, our underwater vehicle is trimmed for neutral buoyancy with the center of gravity being equal to the center of volume. Thus, all forces equal out and the equilibrium is indifferent for any orientation. Since all thrusters point in the same direction, both sway and heave are underactuated degrees of freedom. An interface in the PX4 middleware (called motor mixer) decomposes the desired control forces and moments into control signals for the actuators.

A. State Measurement and Estimation

The path controller for HippoCampus is based on the estimated states which an extended Kalman filter (EKF) provides. Currently, the EKF implementation of the PX4 flight control stack is used to return the vehicle's estimated orientation in Euler angles $\boldsymbol{\Theta}_e$ in Tait-Bryan convention and

the vector of angular velocities $\boldsymbol{\omega}$ in $\{\mathcal{B}\}$. The roll and pitch angles are derived from the accelerometer and the yaw angle is derived from the magnetometer (a three axis Hall sensor), while all three axes are smoothed by the MEMS gyroscope. The depth sensor is not yet integrated into the EKF, but delivers an accurate depth estimate z_e for depth control even without filtering. From the analog voltage signal U_p in the range from 0 to 3.3 V and a sensor calibration we derive the following conversion:

$$z_e = 0.32\frac{\mathrm{m}}{\mathrm{V}}(U_p - 0.08\,\mathrm{V}) \ . \tag{5}$$

At the state of this paper, the vehicle is unaware of its absolute position and velocity in x and y direction, but an acoustic localization system has been successfully tested and will be deployed for the presented system. Both, the pressure measurements and the time delays of arrival of the acoustic signals will be integrated into the EKF.

B. Path Controller

We implement a controller that stabilizes the vehicle in a desired orientation and then follows the angular velocities and depth set points which are derived from a given path. The four-thruster-design of this vehicle enables orientation changes while holding the position. Thus, it is necessary to constrain the part of the control action necessary for path following, while the vehicle is not aligned to it. This is achieved with the alignment factor f_a multiplied to the desired forward velocity and yaw rate:

$$f_a(\phi_e, \theta_e, \psi_e) = \left[1 + a_\phi \left|\phi_d - \phi_e\right| + a_\theta \left|\theta_d - \theta_e\right| + a_\psi \left|\psi_d - \psi_e\right|\right]^{-1} \ , \tag{6}$$

which equals one for a perfectly aligned vehicle and is close to zero for an unaligned vehicle, with the tuning parameters $a_{\phi,\theta,\psi}$ for the respective axis. Index $_d$ denotes desired values and $_e$ estimated values.

In order to stabilize the vehicle in a specific state, a controller has been developed. Since the velocity cannot be measured yet, a closed-loop control for the longitudinal direction is not possible. The necessary thrust is derived from the steady state of Eq. (3) for a constant velocity u_d and provided as the desired longitudinal thrust X to the control mixer. The resulting control actions for forward thrust X and all three moments K, M, N read as follows:

$$X_d = \mathrm{k}_u f_a(\phi_e, \theta_e, \psi_e)\mathrm{D}_A u_d^2 \ , \tag{7a}$$

$$K_d = \mathrm{k}_\phi(\phi_d - \phi_e) + \mathrm{k}_p(p_d - p_e) \ , \tag{7b}$$

$$M_d = \mathrm{k}_\theta(\theta_d - \theta_e) + \mathrm{k}_q(q_d - q_e) \ , \tag{7c}$$

$$N_d = \mathrm{k}_\psi(\psi_d - \psi_e) + f_a(\phi_e, \theta_e, \psi_e)\mathrm{k}_r(r_d - r_e) \ , \tag{7d}$$

where $\mathrm{k}_{u,\phi,\theta,\psi,p,q,r}$ are tuning factors for the controller, index $_d$ denotes desired and $_e$ estimated values.

For depth control an outer cascade with proportional feedback provides the desired pitch angle θ_d, which is also dependent on the direction of the forward thrust:

$$\theta_d = \mathrm{sgn}(X)\mathrm{k}_d(z_e - z_d) \ . \tag{8}$$

V. EXPERIMENTS

The basic controls functionality and vehicle dynamics are studied at the test tank of the Institute of Mechanics and Ocean Engineering at Hamburg University of Technology Due to the lack of an absolute positioning system, we test several preplanned trajectories which can be executed with the on-board sensor suite.

A. Path Planning

A basic scenario is an upward winding motion, as illustrated in Figure 6. This helix with radius R and lead L shall be followed by the vehicle with a forward velocity of u_d. From these parameters we can deduct the period of one full

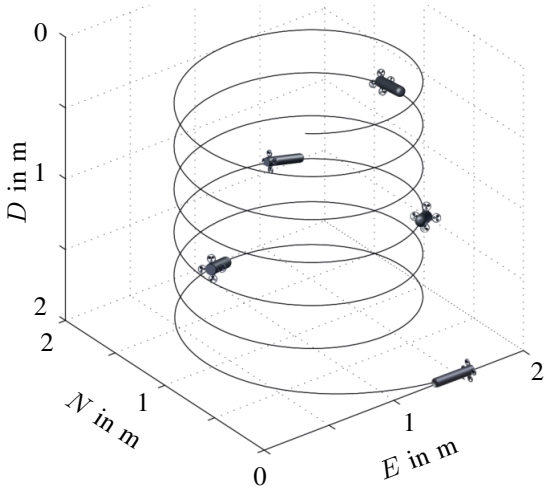

Fig. 6. Desired helical path with a diameter of 1 m and a lead of 0.5 m.

revolution:

$$T = \frac{\sqrt{(2\pi\mathrm{R})^2 + \mathrm{L}^2}}{u_d} \ . \tag{9}$$

Due to the lead L, the pitch angle of the vehicle has to be

$$\theta_d = \mathrm{atan}\,\frac{L}{2\pi R} \tag{10}$$

and the angular rate vector $\boldsymbol{\omega}$ is collinear with the base vector $\boldsymbol{e}_\mathrm{D}$ of the inertial frame $\{\mathcal{I}\}$. In the body fixed frame $\{\mathcal{B}\}$, where this rate is measured and provided by the EKF, it has coordinates in $\boldsymbol{x}_\mathrm{B}$ and $\boldsymbol{z}_\mathrm{B}$ direction:

$$r_d = \frac{2\pi}{T}\cos\theta \ , \tag{11}$$

$$p_d = \frac{2\pi}{T}\sin\theta \ . \tag{12}$$

The desired heading of the vehicle ψ_d and the depth z_d are functions of time:

$$\psi_d = \frac{2\pi}{T}t \ , \tag{13}$$

$$z_d = \frac{L}{T}t \ . \tag{14}$$

The remaining states ϕ_d and q_d shall both be zero:

$$\phi_d = 0 \ , \ q_d = 0 \ . \tag{15}$$

B. Results from Experiments

The vehicle displays a very agile and robust behaviour. The experiments are executed with a trim slightly aft so that the stern of the vehicle rises to the top if no actuators are used. Furthermore, the control actions are restricted to $40\,\%$ of their maximum possible values due to the tight space in the test tank. The preplanned helix path excels as a good test scenario since no absolute localization is necessary and long autonomous runs are possible without human interaction. For circular motions, the drift of the path is usually less than $5\,\mathrm{cm}$ per revolution (cf. Figure 7). The parameters introduced in

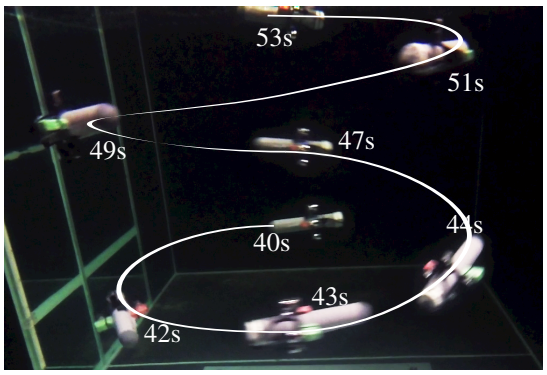

Fig. 7. Helix path from the experiment at times $t = 40\,\mathrm{s}$ to $53\,\mathrm{s}$. See attached video or http://tinyurl.com/tuhh-hippocampus.

Eq. (6) and (7) are tuned during the experiment. A helix path with a lead of $0.2\,\mathrm{m}$ and a radius $R = 0.6\,\mathrm{m}$ shall be followed with a velocity of $u_d = 0.2\,\mathrm{m/s}$. This results in a pitch angle $\theta_d = 0.16\,\mathrm{rad}$, a yaw rate $r_d = 0.97\,\mathrm{rad/s}$, a roll rate $p_d = 0.16\,\mathrm{rad/s}$, and a maneuver duration of $13\,\mathrm{s}$. A video composition of this experiment is illustrated in Figure 7, the logged measurement data is presented in Figure 8 with the upward helical motion from time $t = 40\,\mathrm{s}$ to $53\,\mathrm{s}$. In the first second of the data, the vehicle aligns itself and moves to the desired depth with a left turn. Then it changes direction into a right turn for $180°$ and rises to $z_e = 0.2\,\mathrm{m}$ at $t = 5\,\mathrm{s}$. Afterwards, the direction changes again and the yaw angle ψ_e is decreasing almost linearly for $50\,\mathrm{s}$, first at constant depth, then in a sinking helix. The graph shows that from $t = 40\,\mathrm{s}$ the depth z_e is continuously decreasing. The yaw rate r_e is fluctuating around $1\,\mathrm{rad/s}$, while the roll and pitch rates are a bit jerky. One explanation for the pitch rate fluctuations is that the setpoint for the depth z_d had to be adjusted incrementally in steps of $3\,\mathrm{cm}$, resulting also in the vertical velocity being not as smooth as the controlled yaw angle. Further possible explanations for this behavior are suboptimal gain factors, the dead zone and varying friction of the motors.

At time $t = 53\,\mathrm{s}$, one can see the vehicle penetrating the water surface. This results in a roll angle error of almost $60°$ and in turn, the alignment factor (cf. Eq. 6) is returning a very small value. Thus, the thrust X_d as well as the yaw moment N_d are reduced, while the roll K_d and pitch moments M_d are increasing to realign the vehicle. At the water surface, one rotor is outside of the water and the control action does not return the expected moments and the angular error cannot be compensated.

VI. CONCLUSION

The presented vehicle design outlines a major hardware iteration step in the design towards a modular, agile, and low cost autonomous underwater vehicle. With the intention to build a fleet of five to ten vehicles, the current design shows the capabilities and the problems.

The Pixhawk controller board is the core component of the presented HippoCampus vehicle platform and acts as a central hub for all navigation, measurement, communication, and logging tasks very reliably. The initial results of state estimation and path following are very promising, especially since the implemented controller is in a very early stage and not systematically tuned. Besides a better control structure, improvements in dynamic precision is expected through a stiffer overall design and a correct alignment, fixation, and calibration of sensors and actuators. When the vehicle is trimmed correctly, less control action is necessary and a large disturbing factor is eliminated.

The power to weight ratio of HippoCampus is far beyond the needs of navigating in a test tank. For full thrust without controller aid, keeping the vehicle on a desired path is nearly impossible, and a vertical path from a depth of $1.5\,\mathrm{m}$ upwards results in the vehicle jumping completely out of the water with the center of mass almost one and a half body lengths above the water surface (see Figure 9). Rotations around the pitch and yaw axis can be performed at up to $8\,\mathrm{rad/s}$. This motivates further research in the area of high speed synchronized swarm motions.

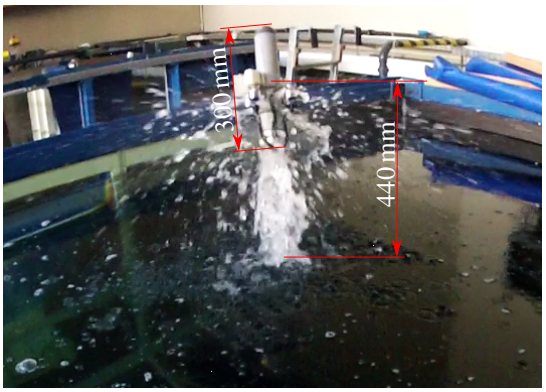

Fig. 9. HippoCampus vehicle jumping $440\,\mathrm{mm}$ out of the water. See attached video or http://tinyurl.com/tuhh-hippocampus.

The next step includes the integration of the acoustic localization system on-board for absolute positioning. When the absolute position is known, trajectory and path following control in an unknown unsteady flow field will be in the focus of research. The ultimate goal of this project is to estimate unsteady flow and temperature fields with a swarm of collaborating autonomous vehicles.

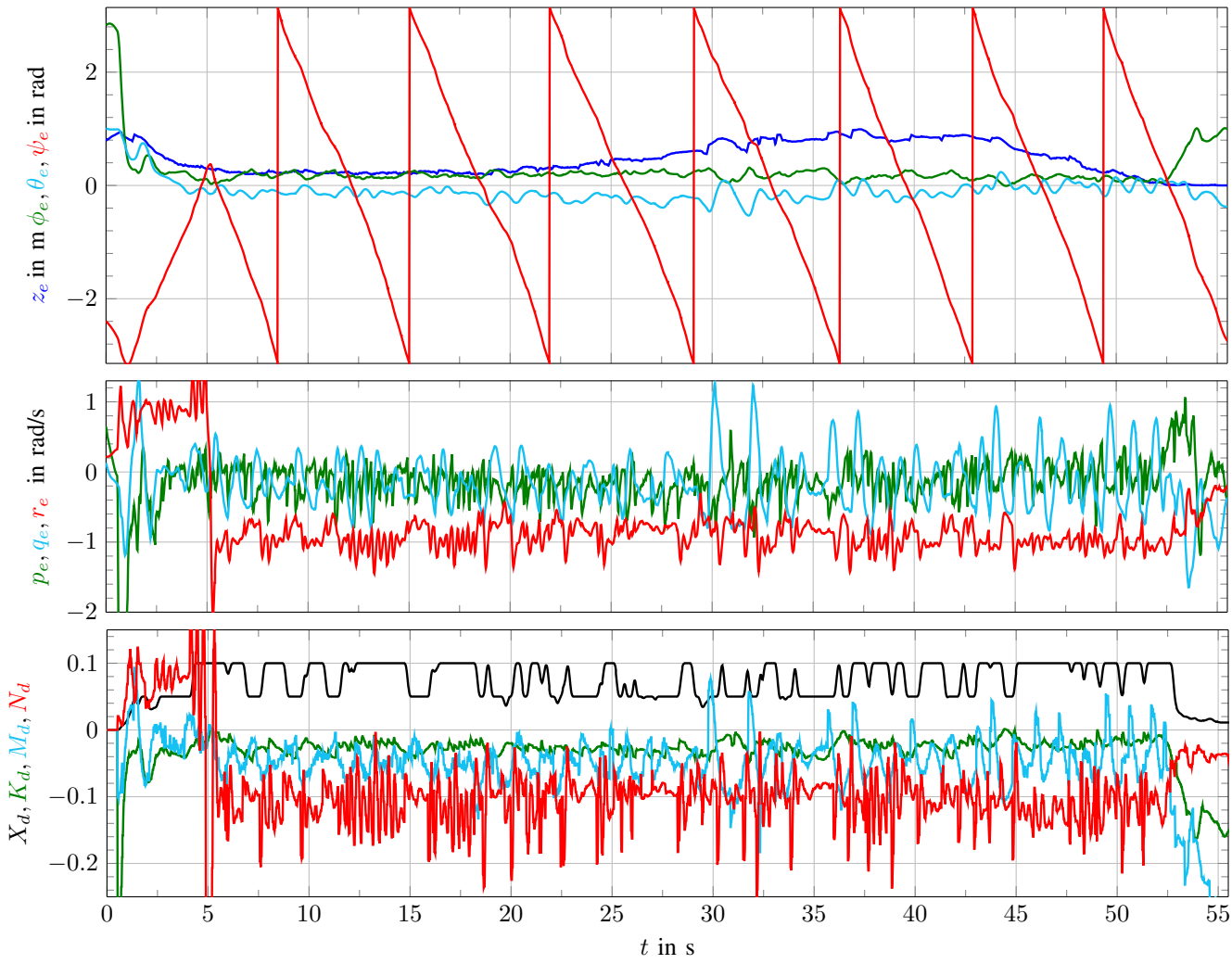

Fig. 8. The illustrated data of the helix path experiment is logged on-board on a microSD card. The upper graph shows depth (z_e ——), roll (ϕ_e ——), pitch (θ_e ——), and yaw (ψ_e ——) angles. The angular rate of change in $\boldsymbol{x}_\mathrm{B}$ (p_e ——), $\boldsymbol{y}_\mathrm{B}$ (q_e ——), and $\boldsymbol{z}_\mathrm{B}$ (r_e ——) directions is shown in the middle graph. Longitudinal thrust (X_d ——) and roll (K_d ——), pitch (M_d ——), and yaw moments (N_d ——), normalized to 1 as the actuator limit, are shown in the lower graph.

References

[1] L. Madureira, A. Sousa, J. Braga, P. Calado, P. Dias, R. Martins, J. Pinto, and J. Sousa, "The light autonomous underwater vehicle: Evolutions and networking," in *MTS/IEEE OCEANS*, Bergen: IEEE, Jun. 2013, pp. 1–6.

[2] K. A. Morgansen, B. I. Triplett, and D. J. Klein, "Geometric Methods for Modeling and Control of Free-Swimming Fin-Actuated Underwater Vehicles," *IEEE Transactions on Robotics*, vol. 23, no. 6, pp. 1184–1199, Dec. 2007.

[3] S. Mintchev, E. Donati, S. Marrazza, and C. Stefanini, "Mechatronic design of a miniature underwater robot for swarm operations," in *Int. Conf. on Robotics and Automation*, Hong Kong, 2014.

[4] C. Osterloh, B. Meyer, A. Amory, T. Pionteck, and E. Maehle, "Monsun II–towards autonomous underwater swarms for environmental monitoring," in *Int. Conf. on Intelligent Robots and Systems*, Vilamoura, Portugal, 2012.

[5] S. Napora and A. D. Paley, "Observer-based feedback control for stabilization of collective motion," *Control Systems Technology, IEEE Transactions on*, vol. 21, no. 5, pp. 1846–1857, 2013.

[6] R. Sepulchre, D. A. Paley, and N. E. Leonard, "Stabilization of planar collective motion with limited communication," *IEEE Trans. on Automatic Control*, vol. 53, no. 3, pp. 706–719, 2008.

[7] G. Hoffmann, J. S. Jang, and C. J. Tomlin, "Multi-Agent X4-Flyer Testbed Control Design: Integral Sliding Mode vs. Reinforcement Learning," in *Int. Conf. on Intelligent Robots and Systems*, IEEE, 2005, pp. 468–473.

[8] D. Mellinger and V. Kumar, "Minimum Snap Trajectory Generation and Control for Quadrotors," in *Int. Conf. on Robotics and Automation*, Shanghai: IEEE, 2011, pp. 2520–2525.

[9] S. Lupashin, M. Hehn, M. W. Mueller, A. P. Schoellig, M. Sherback, and R. D'Andrea, "A platform for aerial robotics research and demonstration: The Flying Machine Arena," *Mechatronics*, vol. 24, no. 1, pp. 41–54, 2014.

[10] L. Meier, D. Honegger, and M. Pollefeys, "PX4: A Node-Based Multithreaded Open Source Robotics Framework for Deeply Embedded Platforms," in *Int. Conf. on Robotics and Automation*, Seattle: IEEE, 2015.

[11] D. J. Klein, P. K. Bettale, B. I. Triplett, and K. A. Morgansen, "Autonomous underwater multivehicle control with limited communication: Theory and experiment," in *Workshop on Navigation, Guidance and Control of Underwater Vehicles*, IFAC, 2008.

[12] T. I. Fossen, *Handbook of Marine Craft Hydrodynamics and Motion Control*. Trondheim, Norway: John Wiley & Sons Ltd., 2011, p. 596.